Edge detection with Mie-resonant dielectric metasurfaces

Andrei Komar,[*,†] Rifat Ahmmed Aoni,[†] Lei Xu,[†,‡,¶] Mohsen Rahmani,[†,¶]

Andrey Miroshnichenko,[‡] and Dragomir Neshev[†]

†*ARC Centre of Excellence for Transformative Meta-Optical Systems (TMOS), Research School of Physics, The Australian National University, Canberra, ACT 2601, Australia*

‡*School of Engineering and Information Technology, University of New South Wales, Canberra, ACT 2600, Australia*

¶*Advanced Optics and Photonics Laboratory, Department of Engineering, School of Science and Technology, Nottingham Trent University, Nottingham, NG11 8NS, UK*

E-mail: andrei.komar@anu.edu.au

Abstract

We demonstrate optical image processing technique in the form of edge detection of an object by exploring the angular selectivity of Mie-resonant dielectric metasurfaces. By utilizing a metasurface with hexagonal arrangement of nanodisks, we increase the symmetry of the two-dimensional spatial dispersion and homogeneously filter out the low wave-vector components of an image, resulting in displaying its silhouettes. We examine the effect of both electric and magnetic Mie-type resonances on the spatial dispersion and show that the magnetic resonance provides better edge detection. We also explore the polarization sensitivity of the edge detection process and show that it is polarization independent. Our results shed light on the underlying mechanisms of edge detection with resonant dielectric metasurfaces and open new opportunities for

ultra-compact optical image processing devices, having multiple applications in vision and microscopy.

Human vision is the main source of information that we receive all along our communication with the external world. There are no doubts how paramount is the ability to see images for human species. Our eye can capture an image like it is, without any additional processing. If we capture an image from a camera, and have its digital copy, we may carry out many different fancy changes of it. We can make the image blur, substitute colors, vary brightness, remove or add noise or distortion, and so on. One of such image transformation is the edge detection, which is the ability to enhance the silhouettes of an image.[1] Usually, edge detection or other image processing functions are performed digitally, by computational techniques. Two computational methods for edge detection are the Kernel convolution method (see description in the Supporting Information) and the high-pass spatial filtering in Fourier space (will be explained below). However, when human vision or machine vision by systems with limited computational resources are concerned, the computational approaches are not adequate. In this case, optical image processing techniques are required.

Optically, edge detection can be achieved by spatial filtering of the low wave-vector components in real-time using a 4-f imaging system with an amplitude mask in the center of the Fourier plane. The optical filtering is a passive technique, and the output image already represents the silhouettes of the original object. However, such 4-f optical systems are rather bulky and difficult to implement in miniaturized devices for machine or human vision. Therefore, novel approaches that directly perform spatial filtering of the image without Fourier transforms are required.

The use of nanophotonic devices has recently attracted a lot of attention, as they can offer passive image processing with a much smaller footprint.[2] For example, Zhu *et al.*[3] reported on edge detection of an image by coupling to surface plasmon resonances in a metal film. More recently, plasmonic thin film[4,5] and plasmonic nanoparticle arrays[6–8] have been utilized as spatial frequency filters to enhance the edges of an image, as well as to

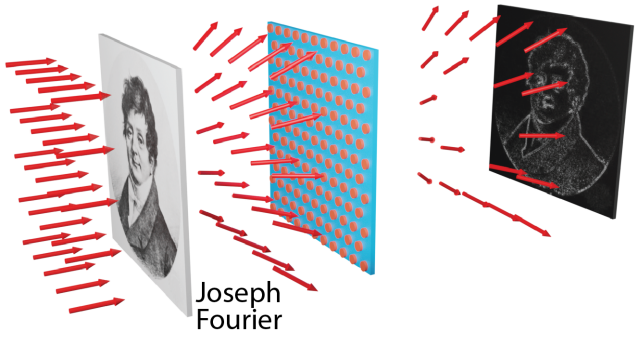

Figure 1: Schematic representation of the edge detection using the metasurface approach, which directly perform spatial filtering of an image without Fourier transforms.

perform phase-gradient detection. However, plasmonic nanostructures exhibit high-intrinsic loss, which places a lower limit on the width of spatial frequency filtering and efficiency of the devices.

Dielectric nanostructures, including photonic crystals and metasurfaces have thereby been put forward to performed more efficient edge detection operation.[9–15] Dielectric metasurface based edge detection techniques have been investigated in one (1D)[10,11,16] or two spatial dimensions (2D).[14,17,18] The 1D grating based approaches are limited to edge detection only in one direction. The 2D dielectric metasurfaces circumvent this issue, however, the polarization sensitivity and angular dispersion of the proposed schemes remains largely unexplored. For example, the broadband scheme reported by Zhu *et al.* employs a regime of strong overlap of two Mie-resonances separated by a bound-state in the continuum mode[12] and as such exhibits polarization dependency and variable spatial filtering at different wavelengths. Therefore, it is of paramount importance to understand the spatial dispersion of metasurface resonances of different nature and achieve polarization independent spatial filtering to enable practical applications in vision technologies.

Here, we experimentally demonstrate dielectric metasurface as an ultra-thin passive element that performs edge detection, as shown in Fig. 1. Our metasurface is based on hexagonal arrangement of silicon nanodisks, exhibiting electric and magnetic Mie-type resonances in the near-infrared spectral region 1400-1600 nm. Due to the resonant nature of

the metasurface and its angular dependent transmittance, low wave-vectors components are filtered while higher wave-vectors can be fully transmitted. We analyze numerically and experimentally the angular dispersion of each of the resonances and compare this angular dispersion and performance for both the magnetic and electric modes of the metasurface. We demonstrate the effective detection of edges in two orthogonal directions and show the polarization independence in the case of the magnetic-resonance. Our results pave the way for multitude of optical imaging applications, including microscopy and navigation for autonomous systems.

Results and discussion

Theoretical framework. We start from the description of a computational method based on Fourier filtering. The mathematical background of this method forms the basis of our passive metasurface edge detection technique. The initial step of that computational method is to perform a Fourier transform of the the image and then filter its low frequencies. The inverse Fourier transform of the filtered spectrum leads to the image which contains only edges, or silhouettes, of image objects. First, let's investigate properties of Fourier filtering. For simplicity we take a 1D function with two sharp edges, a squared step, shown in Fig. 2a. We are going to implement a discrete Fourier transform (DFT), therefore, the function is an array of 100 elements with zeros and ones $\{\mathbf{x_n}\} = (0, 0, 0, \ldots, 1, 1, 1, \ldots, 0, 0, 0)$. DFT is the process that transforms the sequence of in general complex numbers $\{\mathbf{x_n}\} = (x_1, x_2, \ldots, x_N)$ into another sequence of complex number $\{\mathbf{X_k}\} = (X_1, X_2, \ldots, X_N)$ using formula

$$X_k = \frac{1}{\sqrt{N}} \sum_{n=1}^{N} x_n e^{2\pi i (n-1)(k-1)/N}, \tag{1}$$

where, if we speak in terms of signal processing, the numbers $\{\mathbf{X_k}\}$ are frequencies of the initial signal $\{\mathbf{x_n}\}$.

The inverse DFT does an opposite operation transforming complex numbers $\{\mathbf{X_k}\}$ back

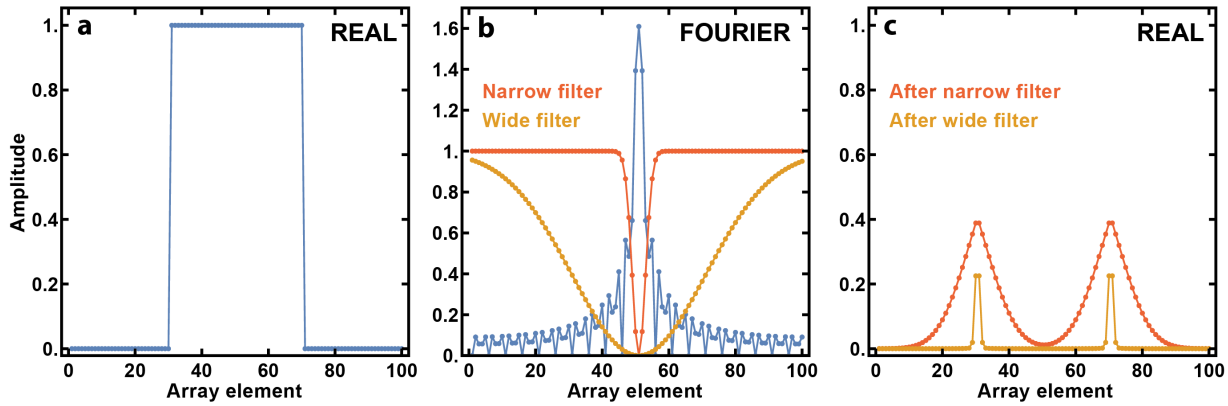

Figure 2: Filtering in Fourier space. (a) The initial signal to process. (b) Fourier spectrum of the signal and two types of filters. (c) The resulting signal after filtering in Fourier space.

into $\{\mathbf{x_n}\}$

$$x_n = \frac{1}{\sqrt{N}} \sum_{k=1}^{N} X_k e^{-2\pi i(k-1)(n-1)/N}. \tag{2}$$

Now, we apply the Fourier transform (eq. (1)) to our signal, and we receive the list of complex numbers, amplitudes and frequencies, of our function in the Fourier space. To demonstrate a Fourier spectrum of our signal, we plot natural logarithm of the absolute values of the amplitudes

$$\ln\left(1 + |X_k|\right). \tag{3}$$

The result is presented in Fig. 2b blue curve. To present the spectrum in a more convenient form, the first frequency is normally shifted to the center of the plot.

Next, we implement high-pass filtering of our spectrum with two filters, narrow (red curve in Fig. 2b) and wide (yellow curve). It means that we multiply our Fourier transform amplitudes at each frequency by filter transmittance values. In this case our first, or in shifted plot, central frequency goes to zero. The difference between narrow and wide filter is the amount of the Fourier spectrum that gets cut. After that, we implement the inverse Fourier transform with a filtered signal to see the result of the filtering. The signals are plotted in Fig. 2c. Both of these filters cut a central frequency which responds for the plain propagation and we observe the edge detection effect. The edges after the wide filter are

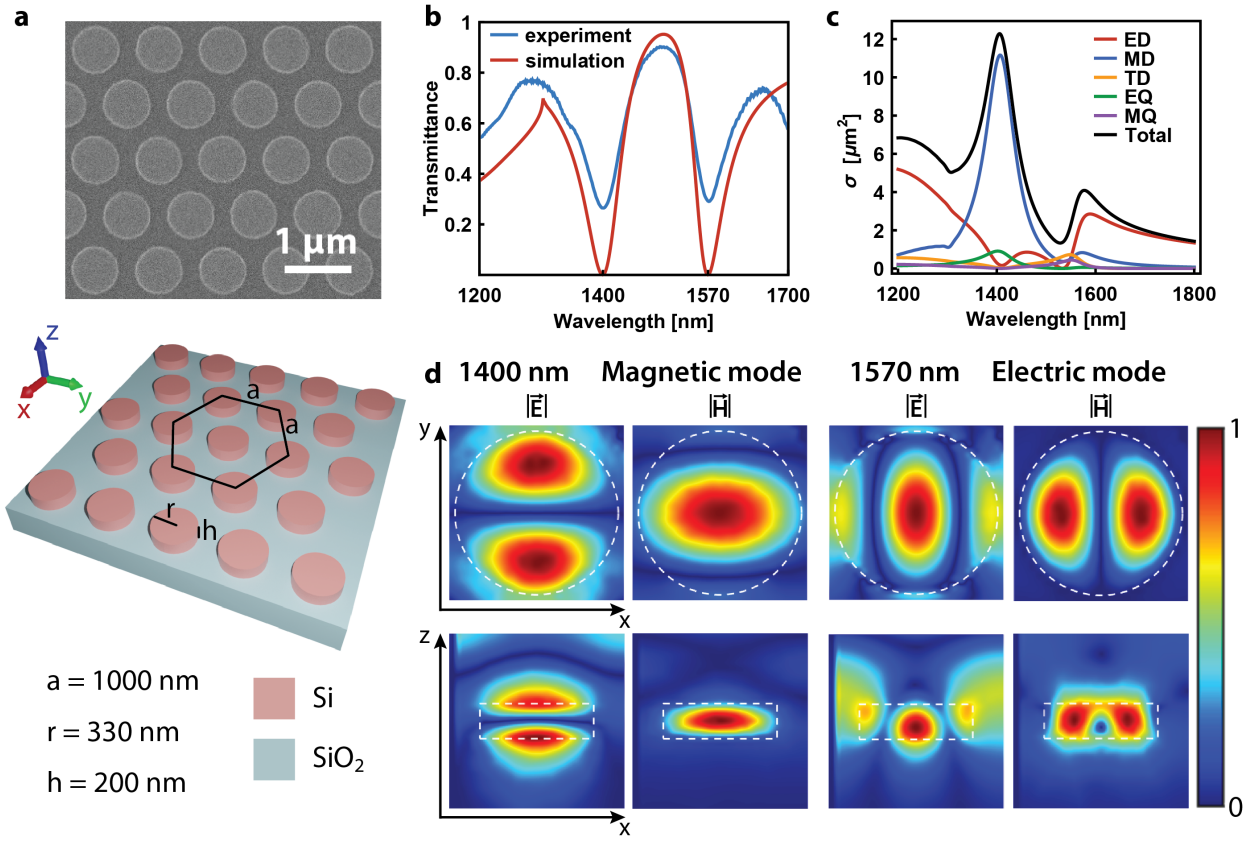

Figure 3: Metasurface parameters. (a) SEM image and scheme with primary dimensions. (b) Simulated and experimental transmittance spectra. (c) Simulated spectral multipole decomposition. (d) Magnetic and electric mode profiles at the resonant wavelengths.

narrower, but with a lower amplitude. The narrow filter cuts less intensity, so the edges are higher by amplitude, but they are wider in space.

What we can expect in the case when our edges in the initial image are not sharp like in the example above? The Fourier filtering result can be approximated by the second derivative of the initial spatial function for the small frequencies, that is the reason why such metasurfaces are frequently named as second order differentiators of a signal or as solvers of integral equations[3,5,9,12] (see the mathematical description in the Supporting Information).

Mie-resonant metasurfaces for edge detection. For the spatial filtering to be effective, we need a metasurface with a sharp resonance feature, which shifts quickly with the angle of incidence. Such property is inherent in dielectric metasurfaces with Mie type resonances. In general, Mie scattering theory is a solution of Maxwell's equations for the

scattering problem of spherical particles with the dimension comparable with the wavelength of the scattered light. The theory is named after the German physicist Gustav Mie. It can be extended for the particles with other than spherical geometry when the separate equations can be written for the radial and angular part of the solution, for example, disks. According to the Mie formalism the incident wave and the scattered field are the sum of the radiating vector spherical harmonics with different amplitude. It was demonstrated that the metasurfaces with the periodically distributed silicon disks, where the sizes of the disks are selected to resonate with the lowest electric and magnetic dipole harmonics, possess the strong angular dependence of a resonance spectral position.[19]

To design such a metasurface, we first carry the numerical investigation using CST Microwave studio with unit cell boundary conditions. The schematic and the SEM image of the metasurface are presented in Fig. 3a. We use a dielectric metasurface composed of amorphous silicon (Si) nanodisks with the radius of 330 nm, the height of 200 nm and the periodicity of 1000 nm. The refractive index of Si is experimentally measured, the results of this measurement are used during the computational investigation. The metasurface has a hexagonal unit cell architecture. The nanodisks parameters are optimized aiming to achieve well-pronounced electric and magnetic responses with a large spectral gap between them and near-zero transmission at the resonant wavelengths. The simulated and experimental transmittance spectra are shown in Fig. 3b, which indicates the well match of resonance wavelengths. To understand the resonance behavior, we have performed the multipolar decomposition of the designed metasurface shown in Fig. 3c. According to Fig. 3c, it is noticeable that magnetic dipole (MD) response is dominant compared to the electric dipole (ED) and other higher order dipoles response. The dominant MD resonance is associated with partly excited electric quadrupole (EQ) resonance at the wavelength of 1400 nm. These results as well as the magnetic and electric mode profiles shown in Fig. 3d prove the Mie-type nature of the resonances and the main multipole contributor to the resonance effect.

Simulation of angular transmittance. We have investigated the angular dispersion

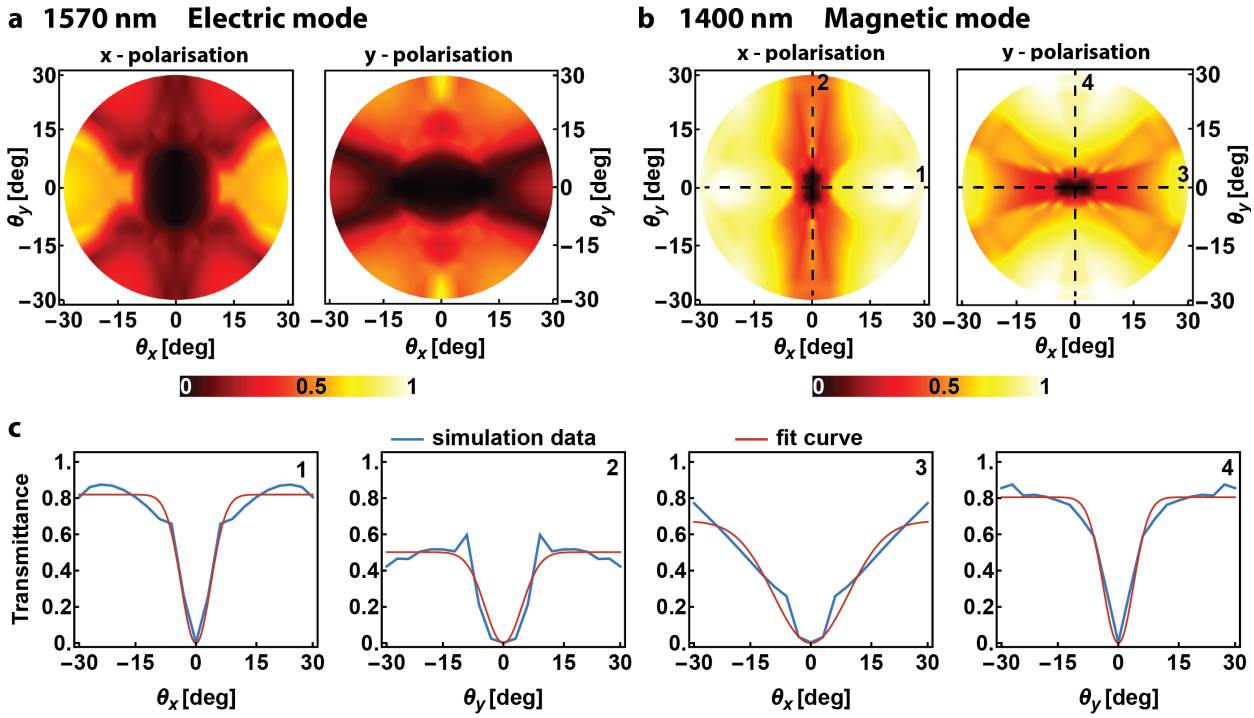

Figure 4: Simulated angular dispersion of the metasurface. (a) Transmittance of the metasurface for different beam angles of incidence at the wavelength of 1570 nm (electric dipole resonance mode). (b) The same transmittance at the wavelength of 1400 nm (magnetic mode). (c) Values of transmittance along the dashed lines in (b) subfigure for magnetic mode along with Gaussian fit of the data.

at the wavelength of the electric and magnetic resonances. All the angular dispersion calculations were carried out using the Lumerical FDTD Suite. The results for electric mode at the wavelength 1570 nm are presented in Fig. 4a, for magnetic mode at the wavelength 1400 nm in Fig. 4b. Each point on the graphs corresponds to the transmittance of the metasurface for particular angle of incidence. The results are presented for both horizontal x-polarization and vertical y-polarization states of light. We have used the periodic boundary conditions. At a specific polarization state (x or y-polarization), we varied the in-plane and out-of-plane azimuthal angles. We varied the out-of-plane azimuthal angles from 0 to 30 degrees with 1 degrees iteration and in-place azimuthal angles from 0 to 360 degrees with 2 degrees iteration.

In real world applications the light will be in most cases either unpolarized, or linearly polarized, that is the reason why we have decided to present our results for linearly polarized

state of light.

The hexagonal arrangement helps to block the smaller k-vectors precisely. Dragomir Neshev: Dear Drago, could you please add some more information about he advantages of the hexagonal lattice? If you find that it is already good, please, delete the comment. Thank you. Furthermore, it helps to achieve the Gaussian type angular dispersion response.

As it was discussed in the introduction of the article, to have the clear edge detection effect, the filter should cut k-space frequencies that respond to the forward propagation of light, the area on the graphs around 0 degree, and the transmittance ideally should resemble the inverse-Gaussian shape. The results show that magnetic response can significantly narrow down the smaller k-vectors components with near-zero transmission. If to use the electric mode as a filter, we see that it also does not transmit the low frequency components, however, the transmittance of the high frequencies is very low as well, therefore, it blocks propagation for all k-space frequencies, that makes such filter impractical for real applications. As a result, we consider the magnetic resonance state for the further investigation. Fig. 4c summarizes the transmittance cross-sections for magnetic resonance along angles in x and y space coordinates for both polarization states. The graphs combine the Lumerical data and the results of Gaussian fitting.

Experimental setup. Now, we move to experimental verification of our metasurface edge detection approach. To demonstrate the effect we should have an image, we name it a target, and by inserting our metasurface filter after the target, we should see the silhouettes of the target on a screen. In the elementary way it is demonstrated in Fig. 1. Our experimental setup, which is shown in Fig. 5, has four major components, source of light, target, metasurface (the edge detection filter), and instead of screen, an imaging camera with a lens at the focal distance.

As a source of light, we use the Chameleon tunable femtosecond laser with the pulse duration of 200 fs and the repetition rate 80 MHz, and the Chameleon optical parametric oscillator (OPO). We need such a sophisticated device only for its tunability feature be-

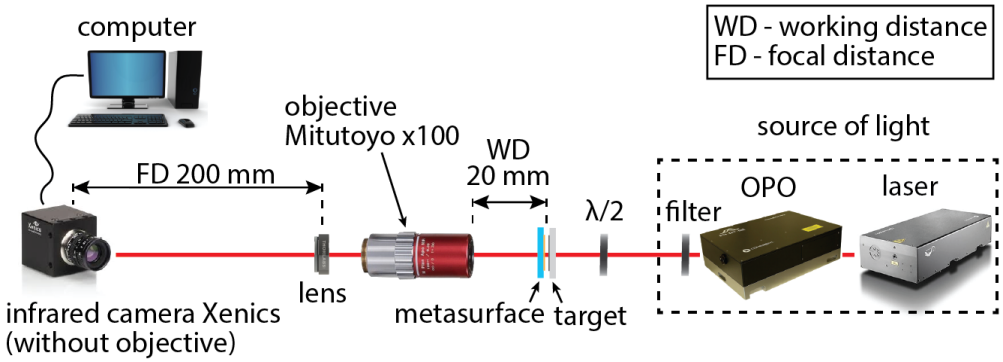

Figure 5: The schematic of the experimental setup.

cause the metasurface approach is a resonance effect, and to have the clear experimental investigation, the wavelength should be tuned to the center of the resonance line and be narrower than its resonance spectral width, that is about 40 nm. The spectral full-width at half-maximum of the laser is 4.4 nm that is satisfy the requirement. A set of filters after the OPO is intended to decrease power to the day light level of several micro Watts because we want to demonstrate the effect as close as possible to the real life application. The edge detection is a linear effect and intensity of light does not play any role unless it is high enough to damage the metasurface.

The beam, emerging from our source of light, is linearly polarized. Therefore, to study the dependence of the edge detection effect from polarization of light, we place a half-wave plate after the light source to rotate the polarization of the incident beam.

After the source of light, we have the target, a R1L3S5P positive Thorlabs resolution test target, which gives us an image, followed by the metasurface at a stage, which we may flip in and out the light pass. We place the metasurface at the closest possible distance from the target. Our metasurface sample is a square with 1 by 1 mm sizes. It means that our target image should be desirably twice smaller in a linear size, about 500 μm, to be able to filter beams with high k-space frequencies (high angles). To see such a small image, we use a Mitutoyo microscope objective with the $\times$100 magnification. As an imaging device, we utilize a Xenics InGaAs infrared camera (XS-1.7-320), which can capture images in the

near-infrared spectral region.

Experimental edge detection. To experimentally investigate the effect, we have chosen the NBS 1963A resolution target as an image for our edge detection verification. The target consists of 5 horizontal and 5 vertical stripes with equal width of the stripes and equal distance between them. As we have already described the overall image size should be less then 500 μm, that is why we have selected the target with 11 cycles per millimeter. It gives as the width of a stripe about 45 μm and the same distance between them. Therefore, 5 stripes uniformly cover 500 μm image size. Fig. 6 presents the experimental results for the edge detection with our metasurface filter. There are two types of 2D intensity distributions in the figure. Image – the captured photos of the target when the filter is out of the light pass, please refer to Fig. 5, and ED (edge detection) – the captured photos when the metasurface filter is flipped into the light pass. It is worth mentioning that no additional alignment is done and no one camera setting is changed when the edge detection filter is incorporated behind the target.

The images with the edge detection filter show the intensity lines only in the position of sharp changes of brightness in the initial images without filter. This is exactly the result we wanted to achieve in our motivation part. The overall intensity of the edge detection images is small, however, this is completely in agreement with the Fourier filtering theory because we cut the high power harmonics. If we looked only at the edge detection image, our eye would adjust the sensitivity to the brightest areas of the image, and the edges would become the most prominent part. If we used a computer to process the edge detection images, we would get the position of the edges of objects just by taken features with the highest intensity in the images. To quantitatively demonstrate the effect, we have plotted the intensities of the pixels along the middle of the images, red lines – for initial image, blue lines – for the edge detection images, for both, vertical and horizontal, stripes.

The effect of the edge detection is observed for magnetic and for electric dipole resonance modes. The theory predicts such behavior. As soon as one cut low frequency spacial modes

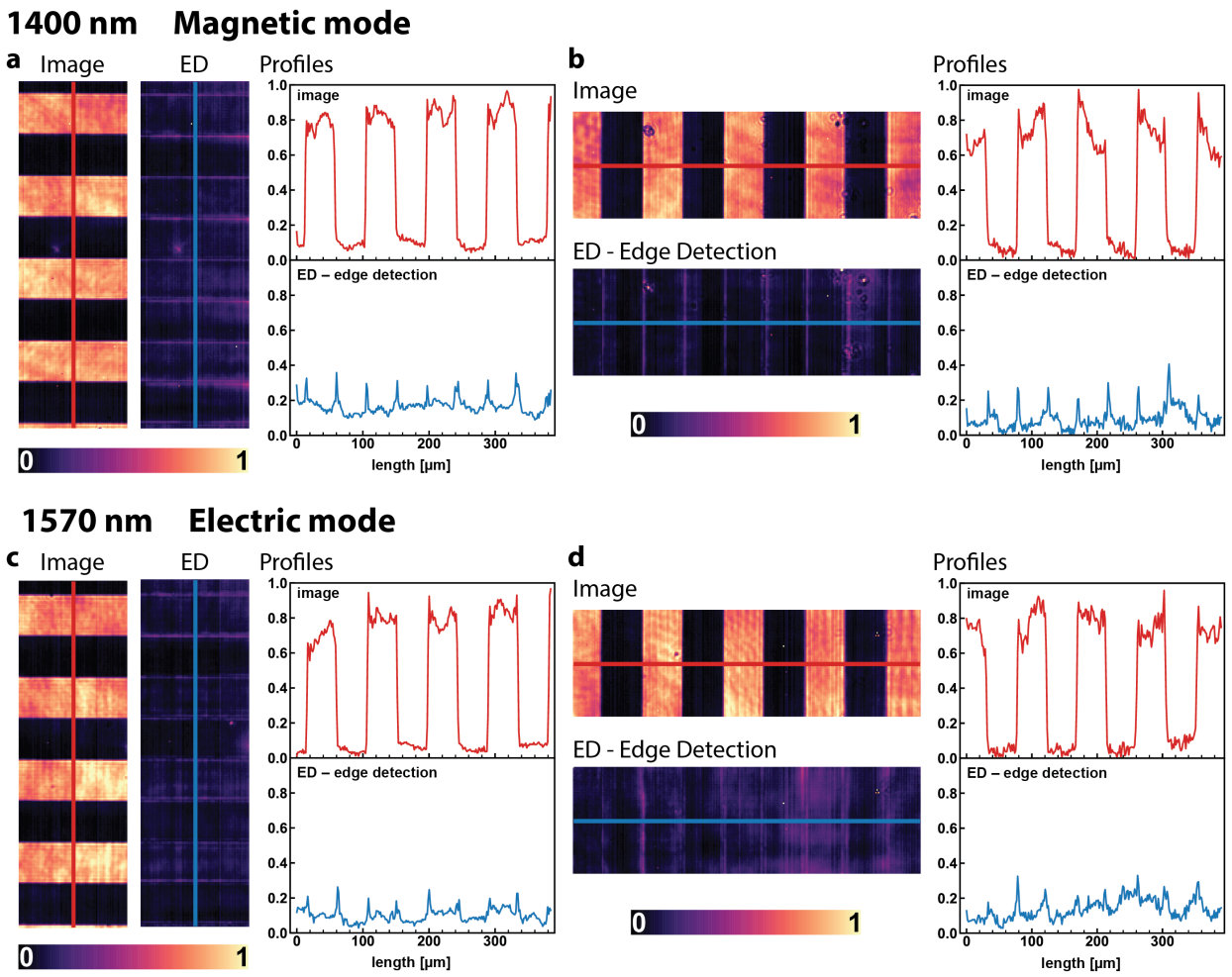

Figure 6: The results of the edge detection experiment. Images and intensity cross-sections for magnetic dipole resonance at 1400 nm for horizontal (a) and vertical (b) stripes, and for electric dipole resonance at 1570 nm (c) and (d).

and even a little transmittance remains for higher frequencies, the edge detection effect is observed. However, in Fig. 6 we see that the effect is more pronounced for magnetic than the electric mode. This is also in agreement with our previous simulations for metasurface angular dispersion, please, compare Fig. 4 a and b results. As we may notice for electric dipole resonance, the transmittance of the high frequency components is very low, it means that the attenuation of the edges will have a sufficient effect.

Polarization independence. In the most application cases the light will be unpolarized. Therefore, we have decided to check experimentally how the polarization of light influences the edge detection efficiency with our metasurface approach. For this experiment

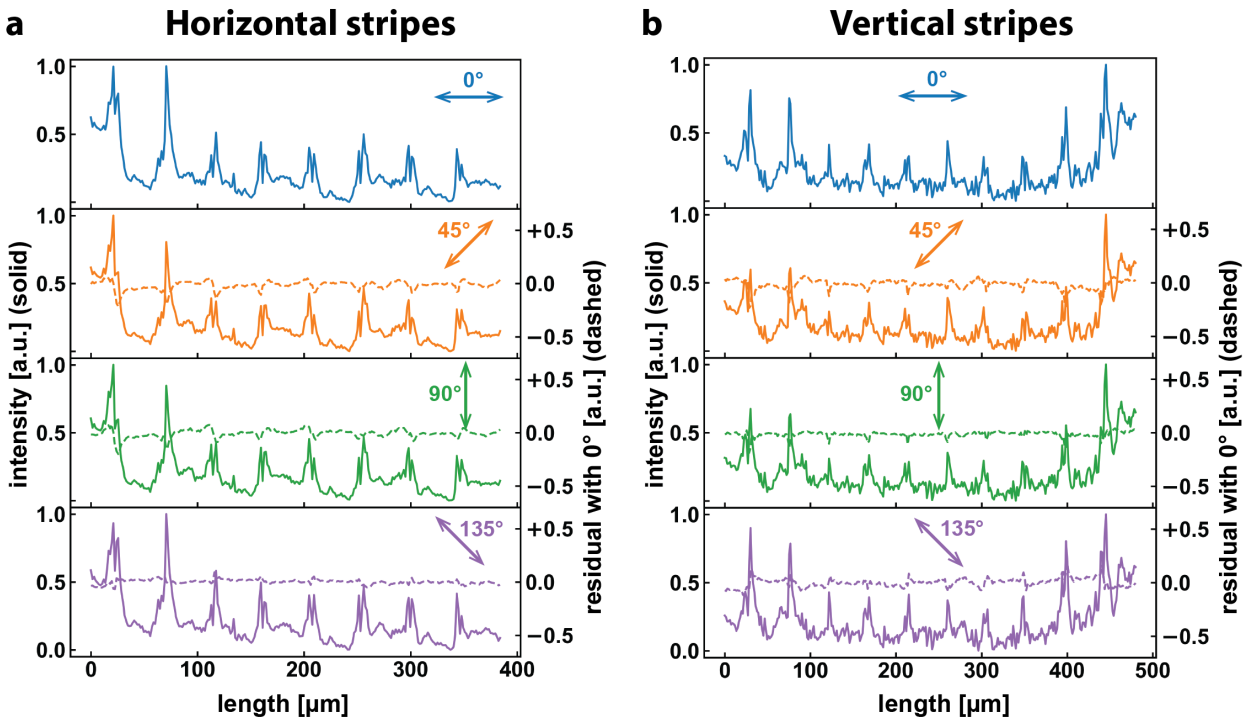

Figure 7: Polarization dependence of the edge detection for magnetic mode dipole resonances. The figure demonstrates the resulting intensity after the metasurface edge detection filter for horizontal (a) and vertical (b) stripes of the NBS 1963A resolution target with 11 cycles per millimeter.

we have introduced a half-wave retarder after the light source, see Fig. 5. The polarization of light after the laser is linear and horizontal relative to the optical table. Rotating the half-wave plate we rotate the polarization of the laser light. Before the experiment we have verified with a linear polarizer that the half-wave plate rotates the polarization and it remains linear for each angle of rotation. We have measured the edge detection effect for magnetic resonance mode, the same as in Fig. 6a and b, for four incident polarization states, 0° (horizontal), 45°, 90° (vertical), and 135°. The results are shown in Fig. 7, for both horizontal and vertical stripes in the NBS 1963A resolution target. This time, we have referenced the intensity to the maximum pixel value for the edge detection result because our goal is to see the variation between different polarizations. The higher intensity at the edges of the target is due to the alignment issues of the overall optical setup. The target and the metasurface sizes are very small and we have to use ×100 objective. For such precise optical system

even tiny misalignment from the absolutely even surfaces leads to the significant effect especially at the areas close to the limits of the objective field of view. However, as soon as the alignment is fixed, we only rotate the polarization of the incident beam, in this case this experiment provides the information about the influence of the different polarizations. As you may see, we have achieved the astonishing results. The edge detection effect is almost the same for all four linear polarization states. This is one of the meaningful properties of our metasurface approach.

Conclusions

We have experimentally demonstrated that by engineering the spatial dispersion of the dielectric metasurfaces we can filter the require k-vectors which provides the efficient edge detection of an object. Our approach is based on the angular dispersion of Mie type dipole resonance. We have investigated theoretically and experimentally both, magnetic and electric, dipole modes and have come to the conclusion that the magnetic mode has better efficiency for the edge detection application. The usage of hexagonal, not square, lattice also improves the angular response of the metasurface. Our metasurface is narrow-band in terms of wavelength of light, however, many applications require or satisfy this limitation. We have experimentally investigated the efficiency of the edge detection for different polarizations of incident light, and have found out that our approach is absolutely independent of the polarization state of light as soon as it is linear. This fact makes our edge detection metasurface an efficient device in the real life applications. We consider that the presented metasurface is already fully functioning optical device if somebody needs the narrow-band passive edge detection element. Due to miniaturize and simple edge detection technique, silicon metasurface will pave the way for optical imaging applications including microscopy and navigation for autonomous systems.

Methods

Simulation. All the numerical investigations have been carried out with Lumerical software with Finite Difference Time Domain (FDTD) solver. The periodic boundary condition has been used towards the x-y directions, while the perfectly match layer (PML) has been applied in z-direction to investigate the scattering response. Plane wave has been used as an excitation source to investigate the response of the device. During the angular transmission analysis, by maintaining the polarization, we varied the in-plane and out-of-plane azimuthal angles. The multipolar decomposition of the disk has also been carried out using FDTD solver.

Sample Fabrication. In this project we have used a thin glass substrate with refractive index n = 1.50, and thickness equals to 170 μm. The glass substrate was cleaned with Oxygen plasma for 10 minutes. By using Plasma-enhanced chemical vapor deposition (PECVD, Oxford PlasmaLab System 100), we have deposited 200 nm amorphous silicon (a-Si) on top of the glass substrate. The expected thickness of a-Si was maintained by checking the a-Si deposition rate with the ellipsometer (JA Woollam M2000D). The optical properties (real and imaginary part of the refractive index) of a-Si were measured using the same ellipsometer. The Diluted ZEP 520 electroresist along with spacer were spin coated for patterning purpose. The samples were then patterned following the standard electron beam lithography (EBL, Raith 150) process with different doses to obtain the expected nanodisk diameters. Next, the development process was performed by inserting the sample into Zep developer. For the masking purpose, 50 nm chromium (Cr) was deposited using Electron Beam Thermal Evaporator (EB Evaporator). Then performed the lift-off process on the sample and etched the a-Si by induction coupled plasma (ICP). Finally, residual Cr mask was removed by the wet etching.

Edge detection images post-processing. All images in our experiments were captured using Xenics infrared camera. The camera has a 14 bits ADC, it means that each pixel has 16384 counts of the intensity range. The camera has such sensitivity that when the laser

is off the average value of pixels intensity is about $4000 - 5000$ counts. To demonstrate the effect of the edge detection in the most convenient way and to be able to compare the level of the edge detection effect correctly, we used histogram approach to scale the color of image presentation. For each experimental image we plotted the histogram of how many pixels has some count value. Utilizing the histogram we can see the dynamic range of our image. We chose the minimum and the maximum count that is presented in the image and used them as cutoff counts to scale the color for better image presentation. The experimental images in Fig. 6 have sample images and edge detection images. Experimentally, the difference is that when the edge detection image was captured the metasurface filter was inserted in the light pass. All settings of the camera remained absolutely the same, and we kept the cutoff counts for the sample images and the edge detection images completely the same. Therefore, we were able to compare correctly and quantitatively the edge detection effect for each experiment. The raw images from the camera, the histograms, and the cutoff counts are summarized in the Supporting Information document.

Acknowledgement

The authors thanks Ann Roberts for the useful discussions. The work was supported by the Australia Research Council, Centre of Excellence and Discovery Projects. The authors acknowledge the use of the Australian National Fabrication Facility (ANFF), the ACT Node.

Supporting Information Available

A listing of the contents of each file supplied as Supporting Information should be included.

- Filename: brief description

References

(1) Sonka, M.; Hlavac, V.; Boyle, R. *Image Processing, Analysis, and Machine Vision*; Cengage Learning, 2014.

(2) Abdollahramezani, S.; Hemmatyar, O.; Adibi, A. Meta-optics for spatial optical analog computing. *arXiv preprint arXiv:2007.14568* **2020**,

(3) Zhu, T.; Zhou, Y.; Lou, Y.; Ye, H.; Qiu, M.; Ruan, Z.; Fan, S. Plasmonic computing of spatial differentiation. *Nature Communications* **2017**, *8*, 15391.

(4) Wesemann, L.; Panchenko, E.; Singh, K.; Della Gaspera, E.; Gómez, D. E.; Davis, T. J.; Roberts, A. Selective near-perfect absorbing mirror as a spatial frequency filter for optical image processing. *APL Photonics* **2019**, *4*, 100801.

(5) Zhang, J.; Ying, Q.; Ruan, Z. Time response of plasmonic spatial differentiators. *Optics Letters* **2019**, *44*, 4511–4514.

(6) Roberts, A.; Gómez, D. E.; Davis, T. J. Optical image processing with metasurface dark modes. *Journal of the Optical Society of America A* **2018**, 1–9.

(7) Saba, A.; Tavakol, M. R.; Karimi-Khoozani, P.; Khavasi, A. Two-Dimensional Edge Detection by Guided Mode Resonant Metasurface. *IEEE Photonics Technology Letters* **2018**, *30*, 853–856.

(8) Davis, T.; Eftekhari, F.; Gómez, D.; Roberts, A. Metasurfaces with Asymmetric Optical Transfer Functions for Optical Signal Processing. *Physical Review Letters* **2019**, *123*, 13901.

(9) Guo, C.; Xiao, M.; Minkov, M.; Shi, Y.; Fan, S. Photonic crystal slab Laplace operator for image differentiation. *Optica* **2018**, *5*, 251–256.

(10) Dong, Z.; Si, J.; Yu, X.; Deng, X. Optical spatial differentiator based on subwavelength high-contrast gratings. *Applied Physics Letters* **2018**, *112*, 181102.

(11) Cordaro, A.; Kwon, H.; Sounas, D.; Koenderink, A. F.; Alù, A.; Polman, A. High-Index Dielectric Metasurfaces Performing Mathematical Operations. *Nano Letters* **2019**, *19*, 8418–8423.

(12) Zhou, Y.; Zheng, H.; Kravchenko, I. I.; Valentine, J. Flat optics for image differentiation. *Nature Photonics* **2020**, *14*, 316–323.

(13) Wan, L.; Pan, D.; Yang, S.; Zhang, W.; Potapov, A. A.; Wu, X.; Liu, W.; Feng, T.; Li, Z. Optical analog computing of spatial differentiation and edge detection with dielectric metasurfaces. *Optics Letters* **2020**, *45*, 2070–2073.

(14) Kwon, H.; Cordaro, A.; Sounas, D.; Polman, A.; Alù, A. Dual-Polarization Analog 2D Image Processing with Nonlocal Metasurfaces. *ACS Photonics* **2020**, *7*, 1799–1805.

(15) Zhou, Y.; Wu, W.; Chen, R.; Chen, W.; Chen, R.; Ma, Y. Analog Optical Spatial Differentiators Based on Dielectric Metasurfaces. *Advanced Optical Materials* **2020**, *8*, 1901523.

(16) He, S.; Zhou, J.; Chen, S.; Shu, W.; Luo, H.; Wen, S. Spatial differential operation and edge detection based on the geometric spin Hall effect of light. *Optics Letters* **2020**, *45*, 877–880.

(17) Ghaleh, S. R.; Ahmadi-Kandjani, S.; Kheradmand, R.; Olyaeefar, B. Improved edge detection in computational ghost imaging by introducing orbital angular momentum. *Applied Optics* **2018**, *57*, 9609–9614.

(18) Zhou, C.; Wang, G.; Huang, H.; Song, L.; Xue, K. Edge detection based on joint iteration ghost imaging. *Optics Express* **2019**, *27*, 27295–27307.

(19) Arslan, D.; Chong, K. E.; Miroshnichenko, A. E.; Choi, D.-Y.; Neshev, D. N.; Pertsch, T.; Kivshar, Y. S.; Staude, I. Angle-selective all-dielectric Huygens' metasurfaces. *Journal of Physics D: Applied Physics* **2017**, *50*, 434002.